A rapid simple approach to quantify chromosome conformation capture

M. Abou El Hassan and R. Bremner*

Genetics and Development Division, University Health Network, Department of Ophthalmology and Vision Sciences, Department of Laboratory Medicine and Pathobiology, University of Toronto, Toronto Western Research Institute, Room Mc6-424, Toronto, Ontario, Canada M5T 2S8

ABSTRACT

Chromosome conformation capture (3C) is a powerful tool to study DNA looping. The procedure generates chimeric DNA templates after ligation of restriction enzyme fragments juxtaposed *in vivo* by looping. These unique ligation products (ULPs) are typically quantified by gel-based methods, which are practically inefficient. Taqman probes may be used, but are expensive. Cycle threshold (Ct) determined using SYBR Green, an inexpensive alternative, is hampered by non-specific products and/or background fluorescence, both due to high template/ULP ratio. SYBR Green melting curve analysis (MCA) is a well-known qualitative tool for assessing PCR specificity. Here we present for the first time MCA as a quantitative tool (qMCA) to compare template concentrations across different samples and apply it to 3C to assess looping among remote elements identified by STAT1 and IRF1 ChIP-chip at the interferon-γ responsive *CIITA* and *SOCS1* loci. This rapid, inexpensive approach provided highly reproducible identification and quantification of ULPs over a significant linear range. Therefore, qMCA is a robust method to assess chromatin looping *in vivo*, and overcomes several drawbacks associated with other approaches. Our data suggest that basal and induced looping is a involving remote enhancers is a common mechanism at IFNγ-regulated targets.

INTRODUCTION

Chromatin is highly dynamic and the conformation of individual loci and/or large domains is linked to nuclear events such as transcription, replication, repair and recombination (1,2). Reorganization of chromatin brings genes to favorable transcriptional domains, and involves looping at individual loci, or multiple co-regulated clusters of genes (3–16). Microscopic assays are suitable for studying chromosomal level movements (17–19), but do not reveal events at the gene level. Chromosome conformation capture (3C) was first developed in yeast (20) and is currently the standard method for studying DNA looping and compaction in mammalian systems with high resolution (7,8,21). 3C is based on formaldehyde cross-linking of chromatin segments that are physically connected (Figure 1A). Cross-linked chromatin is digested with a restriction enzyme, diluted, and ligated, a process that favors intramolecular ligation between chromatin fragments attached during cross-linking due to their proximity *in vivo*. This procedure generates chimeric DNA templates which, for simplicity, we refer to as unique ligation products (ULPs). ULP concentration is proportional to the frequency of looping between the ligated DNA sites and is detected by PCR (Figure 1A).

Quantification of ULPs is central to the correct interpretation of 3C data. ULPs are generally quantified on gels (7,10–16,20–22), which is laborious, subject to error during gel loading and has a narrow linear range. Alternatively real-time Taqman PCR has been used recently to quantify ULPs (23–25). However, Taqman probes are costly; a major issue given that 3C usually involves assessment of multiple positive loops and many negative controls. Also, repeats are a common feature of regulatory elements (26,27) and could make the design of primers plus an internal fluorescent probe problematic. Probes are also sensitive to pH and solution purity, which is a concern in 3C analysis (23). A third approach could be SYBR Green-based quantification. A typical SYBR Green assay consists of two stages: amplification and melting curve analysis (MCA), also know as dissociation curve analysis. During the amplification stage SYBR Green molecules bind to the amplified double-stranded PCR products producing fluorescence, which progressively increases as the reaction proceeds. The cycle number at which the fluorescence starts to increase
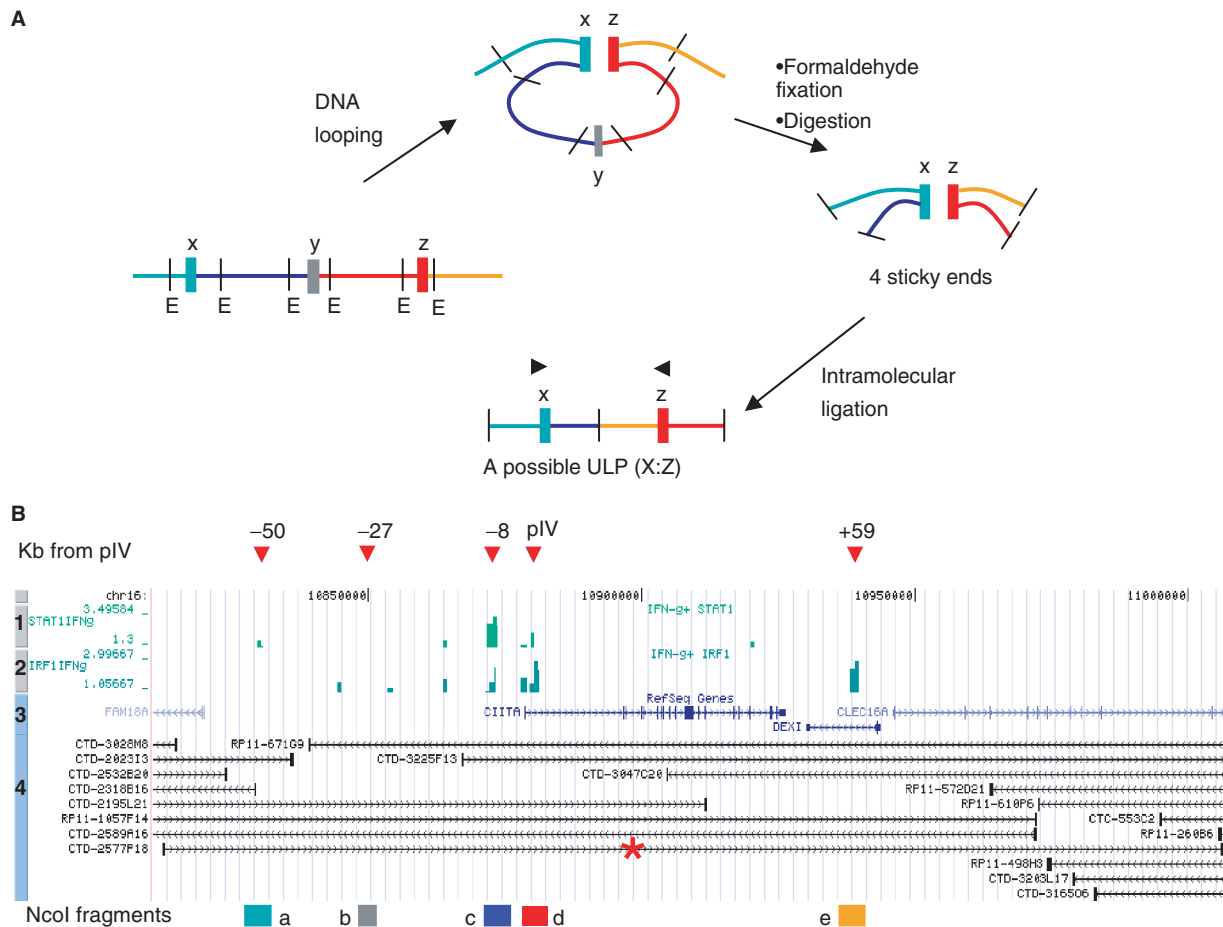
Figure 1. 3C at the *CIITA* locus. (**A**) The 3C procedure. At this hypothetical locus, sites X and Z, but not Y, interact. The X:Y connection is formaldehyde-fixed, digested with a suitable restriction enzyme (E, NcoI in case of the *CIITA* locus) and intra-molecular ligation, favored over inter-molecular ligation by diluting the sample, produces ULPs (X:Z but not X:Y or Y:Z). For simplicity, only one of the potential ULPs is shown. ULPs are detected by PCR using specific primers (black arrows). (**B**) The *CIITA* locus. A 197 kb segment encompassing chr16:10 810 556–11 007 077) is shown. The four tracks in the browser snapshot display ChIP-chip profiles of IFNγ induced binding of STAT1 (Track1) and IRF1 (Track 2), and the location of Refseq genes (Track 3) or BACs (Track 4). BAC (CTD–2577P18, indicated as asterisk) was used in this study. Distance in kb from pIV of various sites and the Nco I fragments used to study bULPs or gULPs (a–e) are indicated above or below the browser window, respectively.

exponentially is called the cycle threshold (Ct) and is used to quantify PCR templates. Calculating the Ct of ULP templates is not possible because the high ratio of total 3C template DNA to individual ULPs (23) creates background fluorescence, and can also favor the formation of spurious PCR products that SYBR green-based methods cannot distinguish from the specific product.

Separate from and subsequent to Ct determination, MCA is typically performed at the end of the PCR to assess specificity. The temperature is increased gradually to melt DNA fragments according to their specific melting temperatures (T_m). The melting of each DNA fragment results in a sudden reduction in fluorescence. Plotting fluorescence negative first derivate ($-dF/dT$), versus temperature generates the characteristic melting curve. MCA is an important and widely applied qualitative tool to distinguish alleles in medical diagnostics and genotyping (28–31). However, some studies have also suggested it may be valuable as a quantitative tool (qMCA). For example, the ratio of the melting peak heights of two

products in the same sample has been used to quantitatively compare the internal ratios of unmethylated versus methylated DNA, two distinct alleles, or two splice variants (32–34). However, it has not been established whether peak height can be used to quantify the amount of two or more target DNAs in distinct samples (such as ULPs from different 3C reactions), and the range over which peak heights for different samples are linearly related to starting template amounts is also unknown. If peak height could be applied in this way it would simplify the design, speed the analysis, and reduce the cost of 3C.

IFNγ triggers phosphorylation, dimerization and nuclear translocation of the transcription factor STAT1, which induces expression of multiple target loci. One target is *IRF1*, itself a transcription factor, which together with STAT1 induces expression of secondary IFNγ target genes (35,36). One important secondary target is class II transactivator, *CIITA*, the master regulator of MHC class II expression (37,38). In addition to binding to the IFNγ *CIITA* promoter (pIV), STAT1 and/or IRF1 bind

to several remote sites around *CIITA* (Figure 1B) (9). To test MCA as a tool to quantify 3C we focused on this locus. An *in vitro* strategy using bacterial artificial chromosome (BAC)-generated ULPs (bULP) revealed that MCA peak position and height could reliably identify and quantify the correct PCR product and was more accurate than a gel-based approach. Analysis of genomic ULPs generated from cross-linked chromatin *in vivo* generated easily identifiable peaks with the same T_m as the corresponding bULPs, and provided linear detection of gULPs from 0.02 to 1.3 pg (BAC equivalence). Our analyses confirm the utility of this simple approach to quantifying 3C templates.

MATERIALS AND METHODS

3C

3C was performed as described (7,20,22,23). Briefly, human adenocarcinoma SW13 cells, grown as described (39), were transduced with the adenoviral vectors Ad-FG or Ad-FG-BRG and exposed to 0.1 µg/ml of human IFN-γ (BioSource International) for 6 h. Cells were cross-linked with 2% formaldehyde for 10 min at room temperature. The reaction was quenched by adjusting to 0.125 M glycine. SDS was added to a final concentration of 0.1% and incubated at 37°C for 10 min to remove any non-cross-linked proteins from the DNA. To sequester SDS and allow subsequent restriction digestion, Triton X-100 was added to a final concentration of 1%. The DNA was digested with NcoI for overnight at 37°C. The restriction enzyme was inactivated by adjusting to 1.6% SDS and incubation at 65°C for 20 min. Digested nuclei were diluted in the ligation buffer to a final concentration of about 3 ng DNA/µl, adjusted to a final Triton-X concentration of 1%, and incubated for 1 h at 37°C. T4 ligase was added and gULPs generated over night at 16°C. The cross-links were reversed overnight at 65°C in the presence of 5 µg/ml Proteinase K and the DNA was purified by phenol–chloroform extraction and ethanol precipitation. Total DNA was quantified by Picogreen dsDNA Quantitation Kit (Invitrogen) and the concentration was adjusted to 50 ng/µl. A no-ligase control was performed in parallel.

Standards for 3C were generated from BAC DNA as described (40). In brief, 30 µg of CTD-2577P18 BAC DNA, covering the *CIITA* locus (Figure 1B), were digested with 300 units of NcoI overnight at 37°C. DNA was phenol/chloroform extracted and ethanol precipitated. A high concentration of DNA fragments (300 ng/µl) were ligated with T4 DNA ligase thus generating equimolar amounts of all possible bULPs. DNA was purified by phenol-chloroform extraction and ethanol precipitation. Calibration samples from 0.00002 to 4 ng total DNA/µl were prepared with(out) 200 ng crosslinked and NcoI digested genomic DNA to cover the dynamic range of detection of all amplified bULPs.

qPCR and standard curve preparation

PCR was performed using an Applied Biosystems PRISM 7900HT using SYBR Green PCR master mix (Applied Biosystems) according to the manufacturer's instructions. We used rapid two-step PCR (35 cycles of 95°C for 15 s and 57°C for 30 s) to minimize non-specific products. MCA was added at the end of each PCR reaction to confirm the specificity of the PCR and determine the specific T_m of each product using ABI Prism 7900 SDS Software (Applied Biosystems). Several primer pairs were tested for each of a selected number of possible ULPs (Figure 2). Preferred primers for a particular locus display similar efficiencies and amplify non-specific products either not at all or only weakly (Figure 3). For a summary of primers used see Table 1. In most cases primers produced one melting peak, although some weak primer dimer peaks were seen (see Results section). PCR products were confirmed by gel electrophoresis. All products were gel purified using Qiagen Gel Extraction kit (Qiagen). A portion of the purified product was used for a second MCA, without repeating the PCR, to confirm the T_m of the specific peak. The remainder was used to confirm the integrity of the PCR products sequencing. Standard curves for each bULP were constructed by plotting the peak heights ($-dF/dT$) versus the log concentration of the calibration samples. The regression coefficients (R^2) and slopes of standard curves were calculated. To compare the MCA with agarose gel quantification, all PCR products analyzed by PCR were also run on 1.5% agarose gels. Specific band densities of calibration samples of each primer were quantified using Gel Doc 2000 (Bio-RAD). Standard curves were constructed by plotting the band density (CNT/mm²) as a function of the log concentration. R^2 values and slopes were calculated. To evaluate the goodness of fit of MCA and agarose gel standard curves, the sum square of residuals (SSR) was calculated as shown in Equation (1):

$$SSR = \sqrt{\sum \left(\frac{y_i - \bar{y}_i}{\bar{y}_i} \right)^2}. \qquad \textbf{1}$$

where y_i and $\bar{y}_i$ indicate the observed and predicted values, respectively, at a concentration *i*.

MCA of gULPs

Total 200 ng of 3C DNA were used in each qPCR reaction as previously reported (7–9). For each PCR reaction a full set of BAC calibration samples was included. Peak heights were normalized twice. First the concentration of gULP under investigation (gULP$_i$) was calculated by calibrating the corresponding peak height to its standard curve [Equation (2)] to correct for differences in PCR amplification efficiencies between primers.

$$gULP_i \text{ concentration} = 10^{(gULP_i \text{ peak height} - c_i)/a_i} \qquad \textbf{2}$$

where a_i and c_i indicate the slope and intercept of the gULP$_i$ standard curve, respectively.

Second, to control for general changes in chromatin status under different conditions (23,41), the concentration of a gULP$_i$, reflecting the looping frequency of the corresponding chromosomal segments, was normalized to
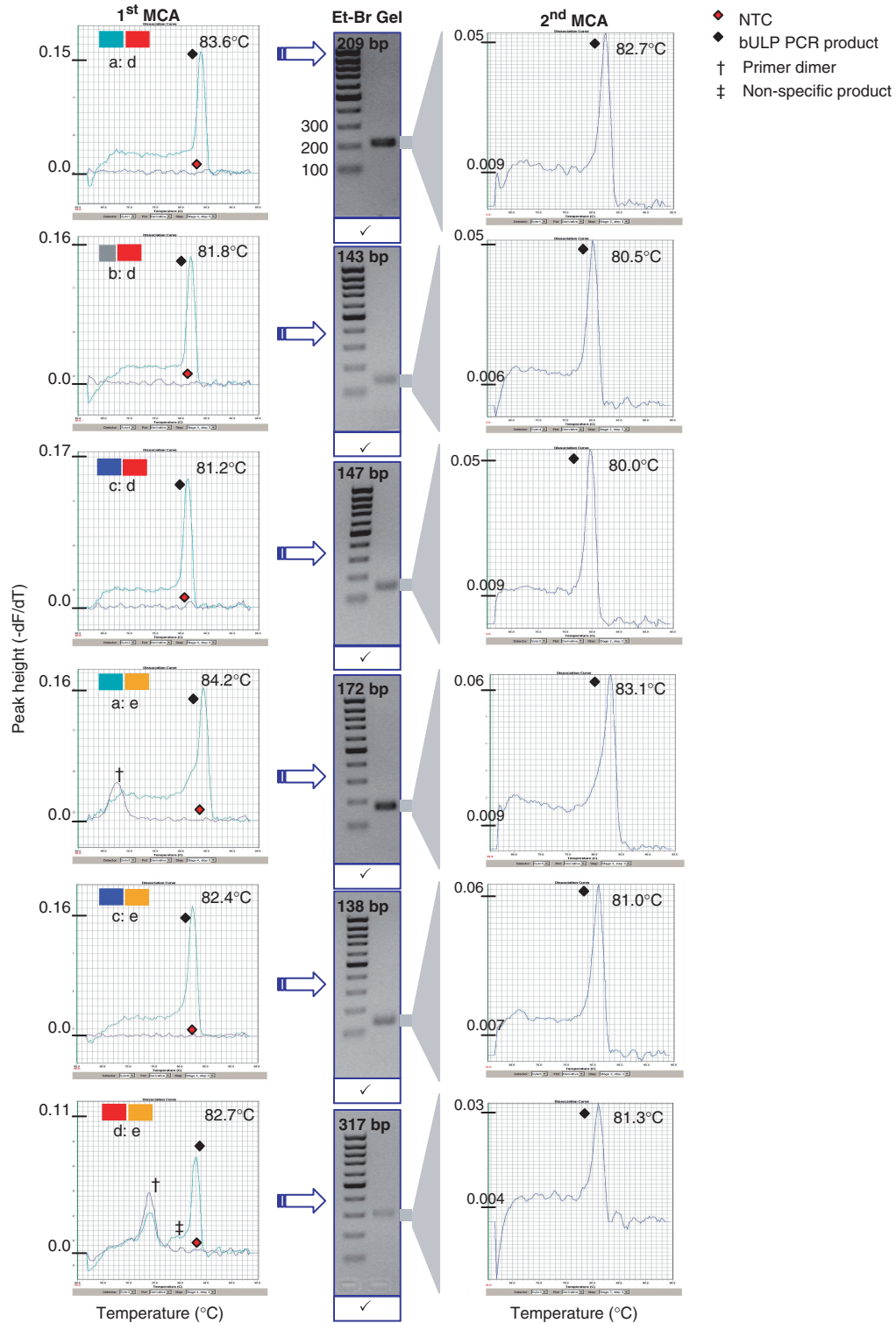
Figure 2. MCA specifically detects bULPs. CTD–2577P18 BAC, covering the *CIITA* locus, was Nco I digested, ligated at high concentration, and bULPs generated through ligation of the indicated Nco I fragments were examined using PCR and MCA performed. Plots on the left show the first MCA, and those on the right show the second MCA after purification in 1.5% agarose gels, displayed in the centre (expected fragment size is indicated at the top of the gel). Half of the gel-purified DNA was used for sequencing and a check mark below the gel indicates that the expected sequence was obtained. Black and red diamonds indicate peaks obtained with the bULP or no-template control (NTC), respectively, and their T_m is indicated. Single dagger signs indicate primer dimers in two samples, and a double dagger indicates another non-specific PCR product in one sample.
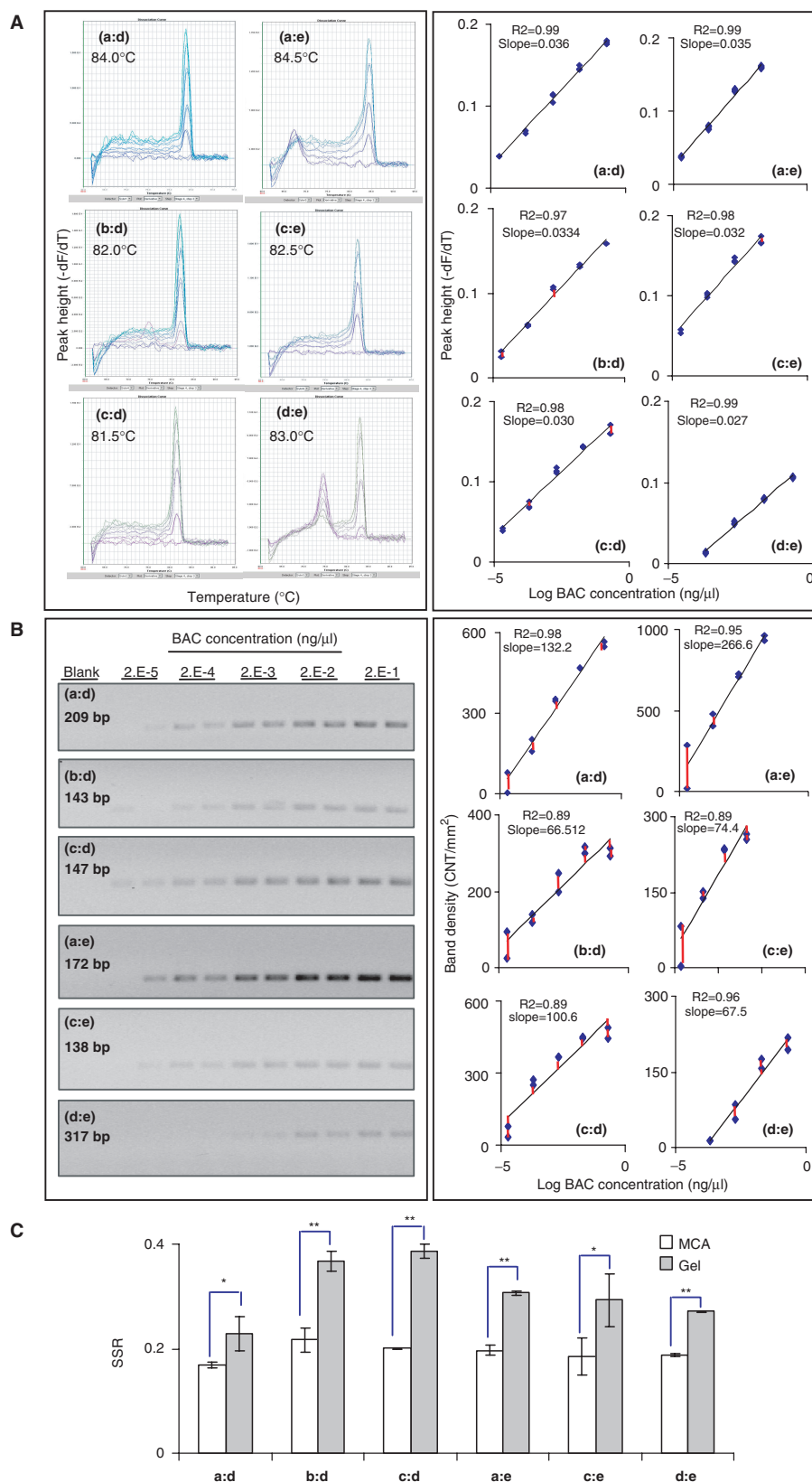
Figure 3. Correlation between bULP concentration and melting peak height or gel band density. CTD–2577P18 BAC was NcoI digested, ligated and 10-fold serially diluted for PCR amplification and MCA. All PCR products were subsequently quantified on 1.5% agarose gels. (**A**) *Left panel*: Representative MCA of bULPs with the indicated T_m values. *Right panel*: Representative standard curves of peak height against log concentration of BAC standard samples. (**B**) *Left panel*: Representative agarose gel images of bULP PCR products. *Right panel*: Representative standard curves of band densities against log concentration of calibration samples. R^2 values and slopes are indicated. Red lines highlight the residuals (difference) between observed and predicted values. (**C**) SSR of MCA and gel-based standard curves for all tested bULPs. Values are the mean ($n = 3$) ± SD. P-values were calculated by Student's t-test: $^*P < 0.05$; $^{**}P < 0.01$.

Table 1. 3C primers

ULPs	Chromosomal location	Primer (5′–3′)	Location	Amplicon length (bp)
a:d	chr16:10 879 952–10 879 971	GTGAAAGTGGCAAACCACCT	*CIITA* pIV	209
	chr16:10 829 457–10 829 476	CGGCTAGGTCACTTTCTCTA	*CIITA* −50 kb	
b:d	chr16:10 852 818–10 852 839	TATCTACAGGTCACTTTCCAGG	*CIITA* −27 kb	143
	chr16:10 879 951–10 879 970	TGAAAGTGGCAAACCACCTC	*CIITA* pIV	
c:d	chr16:10 872 647–10 872 666	CAACGTGCATGGTGGAAAGA	*CIITA* −8 kb	147
	chr16:10 879 919–10 879 938	GCCCCTGAGATGAGCTAACT	*CIITA* pIV	
a:e	chr16:10 940 710–10 940 736	AATGGGATTGTGTCATCTCCTGCCTAG	*CIITA* + 59 kb	172
	chr16:10 829 450–10 829 476	CGGCTAGGTCACTTTCTCTAGTAGGGA	*CIITA* −50kb	
c:e	chr16:10 940 711–10 940 737	ATGGGATTGTGTCATCTCCTGCCTAGA	*CIITA* −8kb	138
	chr16:10 872 651–10 872 677	GTGCATGGTGGAAAGATGACTGTAAGT	*CIITA* + 59kb	
d:e	chr16:10 940 615–10 940 641	GACAACTAACAGCATCTGAGGTGGTGG	*CIITA* + 59kb	317
	chr16:10 879 972–10 879 998	TCTGTTTCTCTCCAACTCAGTCCAACC	*CIITA* pIV	

the average concentration of a set of control gULPs (gULP$_c$) [Equation (3)].

$$\text{Normalized crosslinking frequency} = \frac{\text{gULP}_i}{\text{gULP}_c} \qquad \mathbf{3}$$

The data was then presented as fold above the normalized cross-linking frequency between the promoter and a site at −27 kb that lacks any chromatin activity (9). The data were reproduced in three to six independent experiments. Changes in the looping frequencies between the different NcoI fragments were statistically evaluated by one-way ANOVA followed by Fisher's test.

RESULTS

Specific detection of bULPs using MCA

MCA is used widely to discriminate qualitatively between multiple variants, for example in genotyping and microbial detection (28,30,42). Here we used MCA as both a qualitative and quantitative tool. To generate a set of initial test templates, a BAC vector covering the *CIITA* locus (CTD-2577P18; Figure 1B) was digested with NcoI, and the resulting fragments were ligated at high concentration to generate all possible ULPs. The chimeric fragments were analyzed by PCR using primers that amplify six bULPs generated from fragments a–e representing the promoter (pIV), three remote regulatory elements and a negative control site at the CIITA locus (9) (Figure 1B). A single peak was observed in four out of six PCR reactions (Figure 2, left panel. bULPs: a:d, b:d, c:d, c:e). MCA of bULPs a:e and d:e revealed extra peaks (single and double dagger signs) in addition to the predicted correct peak (black diamond). Two of the extra peaks represented primer dimers as they appeared in the no-template-control (NTC; Figure 2) and their low T_m values of 68°C and 74°C meant they did not interfere with the a:e and d:e bULP peaks with T_m values of 84.2°C and 82.7°C, respectively. In addition, and only for the bULP d:e, a small shoulder (double dagger) appeared at a T_m of 79°C, which also did not interfere with the correct bULP peak (Figure 2). Thus, MCA

Table 2. A summary of T_m values and linear ranges of detection of bULPs using MCA

ULP	T_m (°C)	Linear range (ng/µl of BAC equivalence)
a:d	83.8 ± 0.6	0.00002–0.2
b:d	81.8 ± 0.4	0.00002–0.2
c:d	81.3 ± 0.7	0.00002–0.2
a:e	84.4 ± 0.5	0.00002–0.02
c:e	82.4 ± 0.6	0.00002–0.02
d:e	82.9 ± 0.3	0.0002–0.2

efficiently separates products based on their T_m, allowing accurate measurement of the specific signal. To validate peaks, PCR products were sized on agarose gels. A single major band was detected at the expected size for all six bULPs (Figure 2; note that any primer dimers were run off the gel in this instance). The minor non-specific shoulder seen in the MCA analysis of d:e did not generate a visible band on the agarose gel indicating the higher sensitivity of MCA (Figure 2). The PCR product was excised, purified, and half was sequenced directly. DNA sequences of all bULPs were exactly those expected (data not shown). With the remaining gel-purified sample a second MCA was performed to confirm that minor non-specific peaks were eliminated, proving the identity of the correctly sized product. Indeed, all gel-purified PCR products generated a single sharp peak with a T_m that was slightly (∼1°C) lower than seen with the unpurified template (Figure 2, compare left and right panels). This marginal difference can be attributed to minor traces of salts in the primary template DNA, known to slightly affect T_m (43,44). The minor shoulder on the d:e plot disappeared from the second MCA, confirming it as a non-specific product. We then checked the stability of T_m of all tested PCR products and found that their values, which ranged from 81.3 to 84.4°C, were highly stable and showed high reproducibility between experiments (Table 2). These data suggest that MCA specifically and reliably detects different bULPs.

Melting peak height is superior to gel band intensity for quantifying bULPs

SYBR Green peak height has been used to compare ratios of related templates (e.g. splice variants) in the same sample but not to our knowledge as a quantitative method for comparing PCR products in different samples. Thus, we tested the quantitative value of MCA using a set of bULP calibration samples. A linear relationship was observed between the concentration of calibration samples and the peak height for all six tested bULPs, (Figure 3A). Note that peak height is a derivative($-dF/dT$), so as expected the numerical values of the latter change over a much smaller numerical range (4–6-fold) than concentration (several logs). The amplification efficiencies were comparable for all PCRs and minor differences can be corrected using a set of calibration samples (as below). Hagege *et al.* (23) suggested that a secondary digestion of the DNA circles to create linear template would enhance primer hybridization efficacies and thus PCR efficiency, yet our data show a satisfactory linear amplification over four logs in three out of six cases, and three logs for the other three bULPs with correlation coefficients ≥0.97 (Figure 3A and Table 2). Thus, melting peak height could be used to determine the concentration of bULP with a wide linear range of detection.

Next we compared the use of melting peak height to quantify bULPs with that of the conventional gel-based approach. PCR reactions of all standard samples were run on gels (Figure 3B, left panel) and the density of each band was quantified. Standard curves were constructed in the same range used for SYBR Green detection (Figure 3B, right panel). For each bULP, gel-based quantification produced lower regression coefficients compared to SYBR Green detection and the variability between samples was higher especially at lower template concentrations (Figure 3A versus 3B, right panels). Band densities were not as well distributed around the best fitting line and higher residuals were observed (Figure 3B, red lines). SSR, a measure of the discrepancy between observed and predicted concentrations, confirmed that for all interactions, MCA performed significantly better than gel-based analysis (Figure 3C). Thus, in addition to reducing hazards (EtBr) and effort, MCA improves quantification of ULPs.

Monitoring DNA looping *in vivo*

Having shown that MCA specifically quantifies bULPs (Figures 2 and 3), we asked whether PCR specificity and efficiency is affected under conditions recapitulating the complexity of genomic 3C samples. First we tested the effect of gDNA on PCR specificity by amplifying bULPs in samples containing 0.4 ng/μl of the BAC alone or mixed with 200 ng NcoI digested gDNA, which is similar to the typical amount of 3C template. PCR products were tested by MCA and sized on gels. All products appeared at the expected sizes and T_m values (Figure 4A). In addition, no extra non-specific products or primer dimers appeared as a result of mixing the BAC samples with gDNA. Next, we constructed new MCA-based standard curves using serial dilutions of BAC DNA alone or BAC DNA mixed with

200 ng digested genomic DNA ('mixed BAC'). Increased sample complexity is expected to reduce PCR efficiency, and indeed the peak heights of some PCR products were reduced slightly by the addition of gDNA. Thus, for example, a:e was virtually unchanged while c:d and d:e were slightly affected (Figure 4B). Slopes for BAC versus mixed BAC standard curves were the same, reflecting the expected effect on primer hybridization at the start of amplification (Figure 4B). In addition, there was no effect on the linearity of amplification over a range 0.00004–0.4 ng/μl BAC (Figure 4B). Thus MCA could quantify bULP in complex mixtures with a high degree of specificity and only a modest effect on PCR efficiency in some samples.

Next, we applied MCA-based quantification to *CIITA* gULPs generated by 3C. NcoI fragments a, c, d and e at the *CIITA* locus contain sites of IFNγ-induced STAT1 and/or IRF1 recruitment, while fragment b is a negative control that lacks such binding sites [Figure 1B, (9)]. Ct is measured at the point where PCR becomes exponential, and the relatively high levels of genomic DNA used to quantify gULPs causes fluorescent background that renders Ct-based quantification with SYBR green inaccurate (23,45). However, melting peak height is measured at the end of the PCR, offering a convenient solution.

First, we determined whether gULPs have the same T_m as bULPs. HeLa cells were either left untreated or exposed to IFNγ for 6 h and cross-linked chromatin was NcoI-digested and ligated. The frequency of gULP formation is low (23), thus to ensure reproducible gULP amplification, at least 50–200 ng of 3C DNA were used [this article and (7,21–23)]. Positive signals after MCA were detected for gULPs a:d, linking the STAT1 binding site at −50 kb and pIV; a:e, linking the −50 site to the IRF1 binding site at +59 kb, c:d, bridging the STAT1 and IRF1 bindings sites at −8 kb to pIV, and c:e, joining the −8 kb and +59 kb sites (Figure 5). No signal was detected for b:d or d:e (data not shown) so it was not possible to examine peak height position for these purely theoretical gULPs. The T_m values of all four gULPs detected were similar to those obtained with the corresponding bULPs generated *in vitro* (compare Figure 5 with Figure 4a), and the gULPs ran at the expected size on agarose gels (data not shown). For comparison, we prepared a no-ligase control which lacked gULPs, and in each case the background fluorescence was low (Figure 5). These data show that high amounts of 3C template DNA do not limit the use of MCA in the specific detection of gULPs, and confirm specific amplification of *in vivo* generated gULPs.

As a second test of peak height position, and also to examine the linear range of gULP MCA peak heights, we assessed detection and quantification of *CIITA* gULPs in another cell line. *CIITA* induction requires the chromatin remodeling factor BRG1 (39,46), thus BRG1-deficient SW13 cells were transduced with a negative control adenovirus expressing GFP (AdGFP), or a different adenovirus expressing GFP fused to BRG1 (AdBRG1), and cells were treated with IFNγ for 6 h. Chromatin from treated cells was NcoI digested and ligated at low concentration. Total 200 ng of purified template 3C DNA was used per PCR reaction and six gULPs were assessed, corresponding to
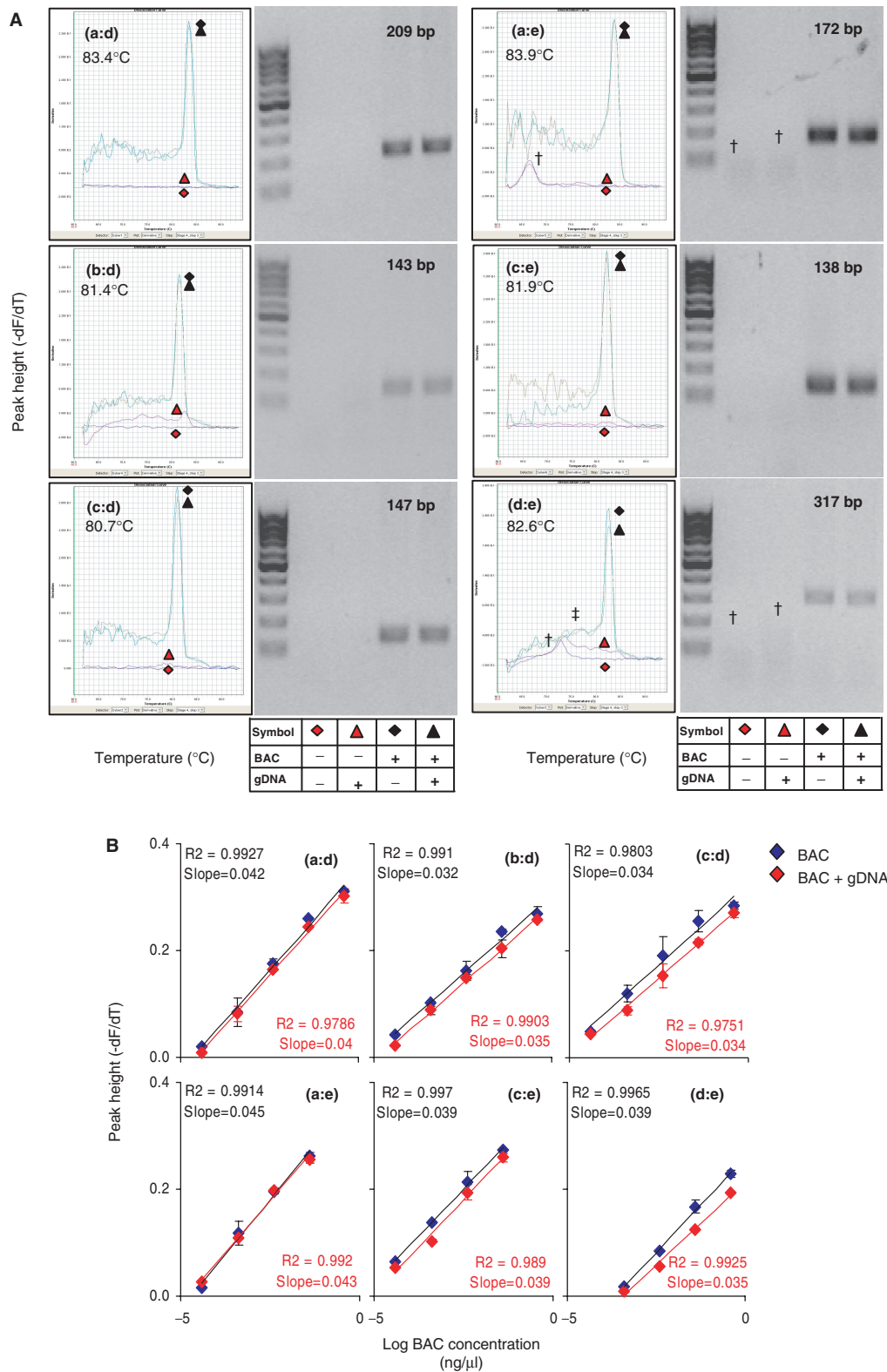
Figure 4. Effects of genomic DNA on amplification of bULPs PCR. (**A**) gDNA does not interfere with PCR specificity. CTD–2577P18 BAC was NcoI digested, ligated and diluted to 0.4 ng/µl alone or with 200ng NcoI digested SW13 DNA. Products were analyzed by MCA (left) and sized on 1.5% agarose gel (right). Tables below the agarose gels indicate the different combinations of BAC and gDNA and the colored diamonds and triangles refer to the melting curve on the corresponding MCA plot. MCA plots are labeled with the ULP name and T_m. Single dagger signs indicate primer dimers, and a double dagger indicates another non-specific PCR product. (**B**) Standard curves of melting peak height against log concentration of BAC alone (blue) or with 200 ng gDNA (red). Curves were constructed from three different data sets. R^2 values and slopes are indicated in black and red for BAC alone or plus gDNA, respectively.
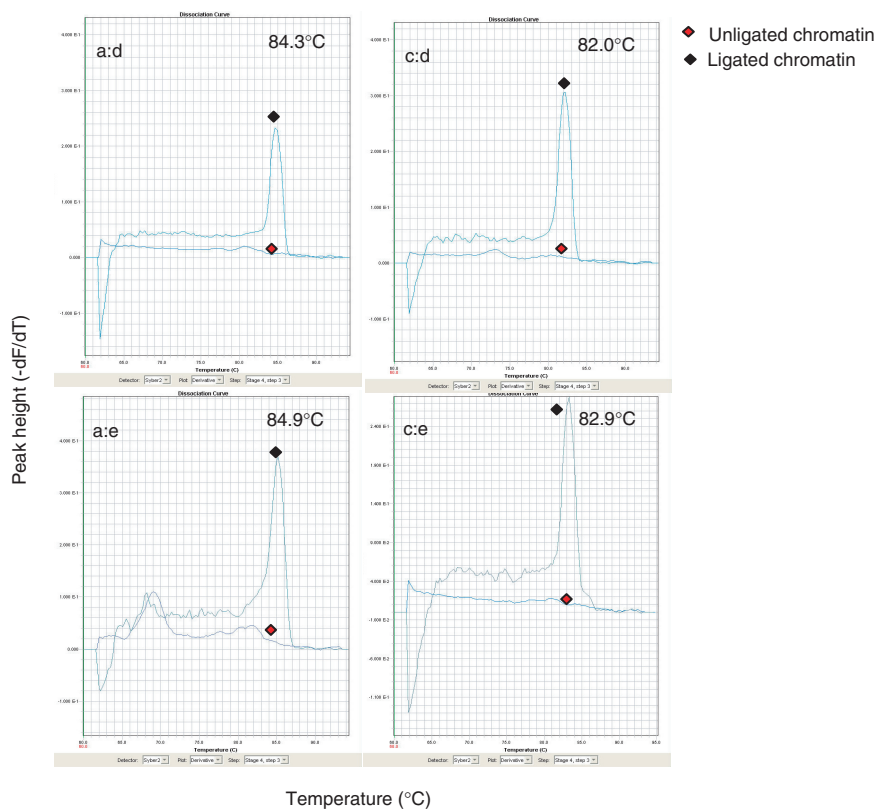
Figure 5. ULPs from HeLa cells. HeLa cells were treated with IFNγ for 6 h, lysed, cross-linked and NcoI digested. Chromatin was purified after overnight incubation with or without T4 DNA ligase. MCA for different gULPs generated low background fluorescence and peaks of the expected T_m (black diamond) that were not detected with unligated cross-linked chromatin (red diamond).

all the bULPs analyzed in Figure 2. As reported for HeLa cells in Figure 4, specific peaks at the expected T_m were detected for a:d, c:d, a:e and c:e (Figure 6A). A marginal peak was detected at the expected T_m for the b:d gULP, consistent with the fact that fragment b is a control region that does not recruit STAT1 or IRF1 (Figure 1). No peak was detected at the expected T_m for the d:e gULP, which was also the case in HeLa cells, suggesting no direct contact between the transcription factor binding sites at pIV and + 59 kb. This gULP did, however, yield a non-specific product at the T_m of primer dimers which was easily distinguished from the d:e PCR product (cf. Figure 6A and Figure. 2). As for the HeLa cell data, each of the specific peaks ran at the expected size on an agarose gel [(9) and data not shown].

Raw peak heights (prior to adjustment using bULP standards) varied between the different gULPs in the order of c:d > a:e, c:e, a:d >> b:d: d:e. *In vitro* analyses above showed that MCA for the corresponding bULPs is quantitative over a large range, either with bULPs alone (Figure 3), or with bULPs mixed with genomic DNA which mimics 3C template conditions (Figure 4). Thus differences in gULP peak height likely reflect real differences in looping frequency. To verify linearity for gULPs we diluted a selection of 3C templates from 200 to 2 ng of 3C template/reaction, equalized the total DNA amount to 200 ng using NcoI digested DNA, and assessed peak height by MCA using equation 2 (see Materials and

Methods section). By definition, it is only possible to titrate gULPs that actually form *in vivo*. Of the six gULPs we assessed in Figure 6A, d:e and b:d were low or absent. In contrast, a:d, a:e and c:e generated moderate peaks, and c:d provided a strong peak. To establish whether MCA-detection of gULPs is linear it is most important to dilute the strongest gULPs since they are most likely to exceed the range of linear detection. Analysis of c:d (the strongest peak) revealed linearity (Figure 6B). One would expect, therefore, that other weaker gULPs would also show linearity. As representatives, we also examined a:e, and a:d and in both cases linear detection was also demonstrated (Figure 6A). In summary, these extensive *in vitro* and *in vivo* analyses of bULPs and gULPs provide considerable confidence that MCA provides linear detection of 3C templates.

Having confirmed that MCA peak heights for gULPs were within the linear range of detection (Figure 6B) we were confident that the observed differences in peak heights between different gULPs either in the presence or absence of BRG1, mirrored genuine differences in the concentration of gULPs. Thus, we calculated crosslinking frequencies of DNA fragments by normalizing peak heights to correct for differences in PCR amplification efficiencies between primers and for possible changes in chromatin status between samples (see Materials and methods section). The complete set of looping data at $CIITA \pm BRG1$ and $\pm IFN\gamma$ is presented elsewhere (9)
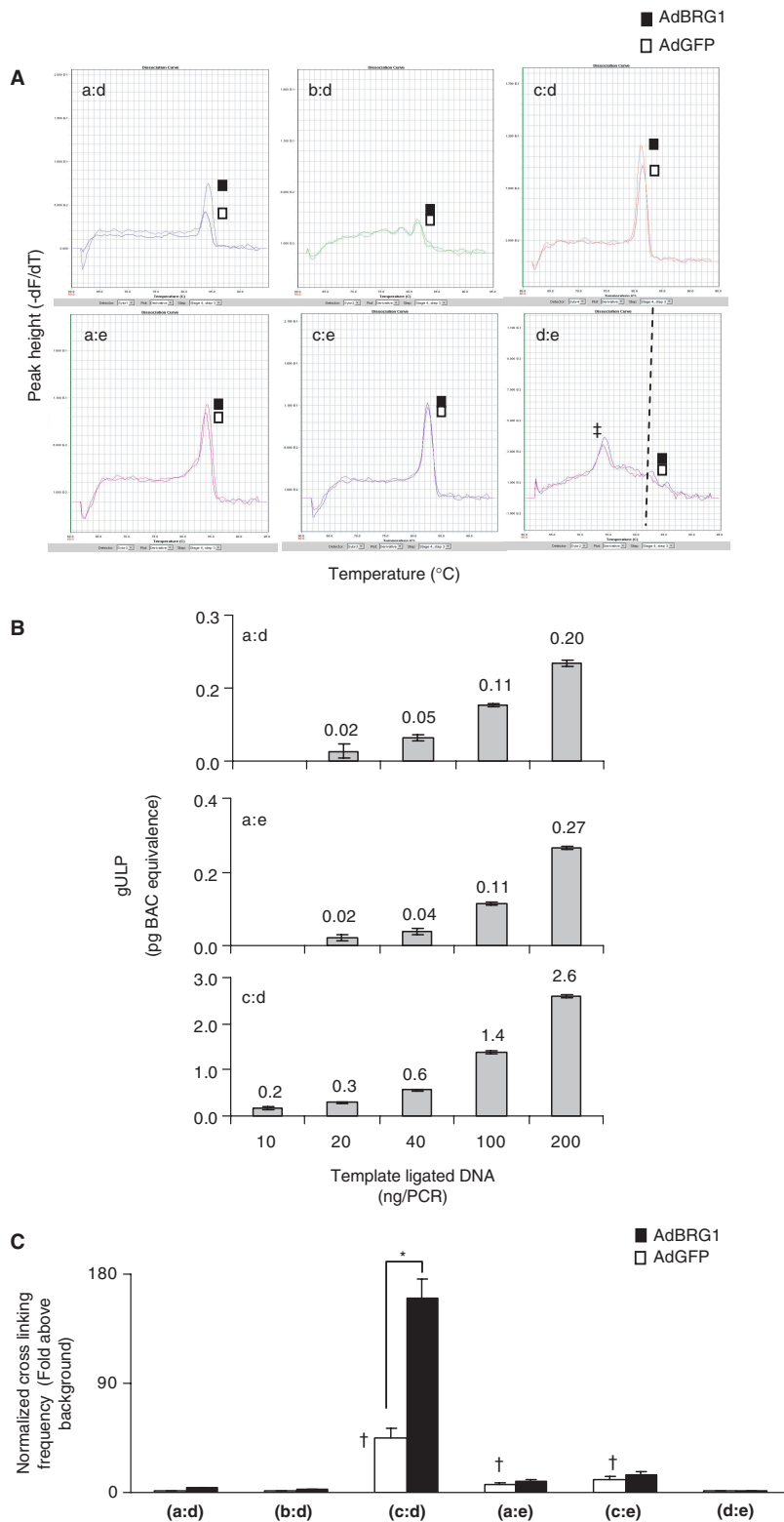
Figure 6. gULPs from SW13 cells and quantification of looping at *CIITA*. (**A**) MCA plots of gULPs generated from SW13 cells transduced with AdGFP or AdBRG1 then exposed to IFNγ for 6 h. Melting peaks appeared at similar T_m values as the corresponding bULPs (Figure 3A). A dashed line indicates the T_m of the d:e gULP, which was hardly detectable. The dagger sign indicates primer dimers. (**B**) Titration of the gULPs a:d c:d and a:e. 3C DNA from the BRG1-reconstituted cells was serially diluted in the range of 0.5–50 ng/μl ligated DNA (2–200 ng per PCR) to determine their linear range of PCR amplification. NcoI digested unligated DNA was added to all dilutions to equalize total DNA to 200 ng/PCR. gULP concentration was calculated in BAC equivalents according to Equation (2) (see Material and Methods section) and was plotted against the concentration of template ligated DNA. Values are the mean of two independent experiments ± range. (**C**) Example of DNA looping frequencies at the *CIITA* locus. Peak heights from (A) were used to calculate the crosslinking frequencies between DNA sites as explained in Materials and methods section. Values are the mean ($n \geq 3$) ± SD. Asterisk indicates significant difference between AdBRG1 and AdGFP while dagger indicates significant basal interaction compared to the negative control b:d. Both asterisk and dagger were calculated by ANOVA followed by Fisher's test.

and revealed several constitutive BRG1-independent loop-ing events, but also that IFNγ-induces additional looping and that these events are BRG1-dependent. Figure 6C shows examples of the looping frequencies in IFNγ treated BRG1-deficient or reconstituted cells. Agarose-based 3C analyses confirms looping events that were detected using MCA (9). Differences in looping frequencies were not arti-facts of proximity of interacting fragments, as shown by multiple control comparisons (9).

In order to further test this approach we used qMCA to study DNA looping at the *SOCS1* locus. *SOCS1* is also an IFNγ target and forms a negative feedback loop to inhibit IFNγ signaling (47). The gene is located ∼380 kb 3′ of the *CIITA* start site. ChIP-chip analysis revealed multiple IFNγ-induced STAT1 and/or IRF1 binding sites around the *SOCS1* locus which were confirmed by ChIP-qPCR (Figure 7A and data not shown). To study possible loops at the locus, HeLa cells were either left untreated or exposed to IFNγ for 6 h and the cross-linked chromatin was EcoRI-digested and ligated. Total 200 ng of the 3C template was used per PCR using specific primers for the ULPs of interest and products were sized on gel and quan-tified by MCA. We did not observe any interaction between the *CIITA* and *SOCS1* promoters (data not shown). A complete description of *SOCS1* looping will be described elsewhere but here we show a subset of the data assessing interaction of EcoRI fragments v:w, w:x, w:y and w:z (Figure 7). Fragment v contains the STAT1 binding site at +50 kb, w includes a STAT1 site at the promoter as well as STAT1 and IRF1 binding sites up to 15 kb downstream, x is 6 kb upstream of the start and showed no STAT1/IRF1 binding, and y and z are STAT1/IRF1 binding sites at −55 and −72 kb, respec-tively (Figure 7A). In untreated cells (basal state) agarose gels revealed bands of the expected sizes for the gULPs v:w, w:y, and w:z, although the middle one was weak, but no band was generated for the negative control w:x (Figure 7B, and data not shown). MCA plots also detected these fragments and, as we had seen above (Figures 2 and 3), MCA was more sensitive as it revealed a weak non-specific product in the w:z amplification that was not visible on the agarose gel (Figure 7B). Both gel-based and MCA analyses revealed that IFNγ treatment increased the amount of v:w and w:z gULPs, but had no effect on the weak w:y gULP and also did not affect the w:x negative control (Figure 7B and data not shown). Normalized cross linking frequencies calculated using MCA data are shown in Figure 7C. Together, these ChIP and 3C data suggest that, as for *CIITA* (9), there are multiple remote enhancers at the *SOCS1* locus that show both basal and IFNγ induced looping to promoter proximal elements.

DISCUSSION

Real-time PCR quantification of 3C ligation products may be hampered by the non-specific fluorescence caused by primer-dimers and/or high concentration of crosslinked DNA templates (23,45). Thus, an alternate but laborious approach is to evaluate gULP concentration by gel-based methods that separate distinct products based on size (7,10–16,20–22). However, this method is impractical for

large scale experiments and is prone to inaccuracy due to the manual errors associated with loading gels.

Recently, Hagege *et al.* (23) used real-time Taqman PCR for the quantification of gULPs at the Igf2/H19 locus. Taqman has some limitations such as the high cost, an important limiting factor for 3C analysis where multiple DNA–DNA interactions are assessed, and gULPs may not always provide ideal sequences for the design of ampli-fication primers together with Taqman probes. Thus, we tested SYBR green and melting peak height as a less expen-sive alternative that does not require a detection probe. Recently, Gudnason *et al.* (48) tested the influence of the concentration and structure of different DNA dyes on the amplification of DNA templates and their melting tem-peratures. They showed that the area under the melting peak using different dyes, including SYBR Green, is pro-portional to the concentration of the template, which agrees with our observation. Others have also shown that the levels of two DNA variants (e.g. splice or allelic var-iants) in the same sample could be quantitatively compared based on their melting peaks (32–34). However, the quan-titative comparison of the same DNA variant but in mul-tiple samples was only done by determining the Ct of each sample, provided that the PCR was highly specific. Use of the Ct method for quantifying ULPs is therefore limited by the non-specific fluorescence of primer dimers and high amounts of 3C template. Here we showed first that the concentration of bULPs in different dilution sam-ples could be quantified using MCA, and that melting peak height offered a wider range of detection than gel-based quantification. We then applied this approach to gULPs. Peaks were detected with the same T_m and fragment size as that seen with control bULPs, and amplification was proportional to the amount of 3C template. Thus, it was possible to quantify looping frequencies between multiple sites at the *CIITA* locus in different cell types, and also at the *SOCS1* locus. The data reveal basal IFNγ-independent looping, consistent with a poised state, which is intensified by IFNγ treatment [this article and (9)].

One of the advantages of gel-based analysis is that, in theory, it visually reveals the presence of non-specific PCR products. However, MCA also exposes non-specific pro-ducts and does so more sensitively than gel based approaches. For example, two out of six bULPs analyzed at the *CIITA* locus had extra peaks by MCA that were barely or not detectable on gels. Importantly, these weaker extra peaks did not interfere with linearity. Thus, not only is MCA-based detection more linear than gel-based detection, it is also capable of detecting even very weak non-specific products. In practice, however, we always test our initial primer sets both by MCA and gel analyses to provide double assurance that there is not a strong secondary fragment being amplified. When non-specific products are detected by both approaches, new PCR primers should be tested.

qMCA is not restricted to 3C ULPs, as we observed similar correlations with genomic DNA templates (unpub-lished data). Thus, the present method expands the utility of SYBR Green qPCR to the quantification of complex looping events, providing a simpler substitute for gel-based quantification of 3C products.
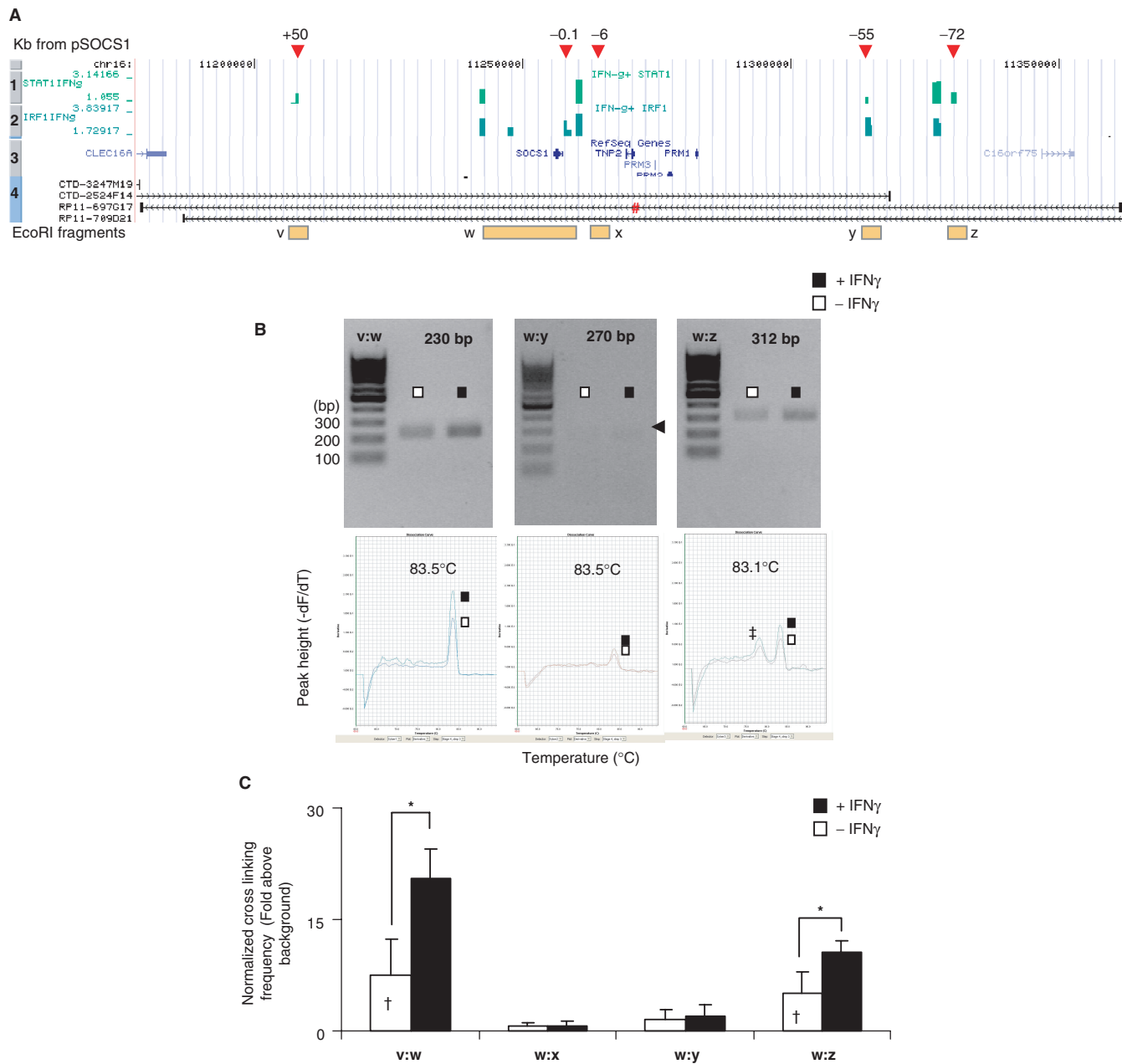
Figure 7. Identification of looping at *SOCS1*. (**A**) The *SOCS1* locus. A 141 kb segment encompassing chr16:11 199 000–11 339 900 is shown. Tracks are labeled as in Figure 1B. The BAC RP11-697G17 (indicated as number sign) was used in the 3C experiment. Distances of various sites in kilo base pairs from the *SOCS1* promoter are indicated by red arrows above the browser window and the *EcoRI* fragments used to study gULPs (v–z) are indicated by boxes below. (**B**) Agarose gels (fragment name and expected size are indicated at the top of the gel) and MCA plots (T_m values indicated at the top of the plot) of gULPs generated from HeLa cells left untreated (open square) or exposed to IFNγ for 6 h (solid square). The double dagger sign indicates a non-specific product. (**C**) DNA looping frequencies at the *SOCS1* locus. Peak heights from (**B**) were used to calculate the crosslinking frequencies between DNA sites. Values are the mean ($n \geq 3$) $\pm$ SD. The dagger sign indicates a significant difference ($P < 0.05$) from the background looping at w:x, and asterisk indicates significant difference ($P < 0.05$) between untreated and IFNγ treated samples. *P* values were calculated by ANOVA followed by Fisher test.

REFERENCES

1. Mostoslavsky,R., Alt,F.W. and Bassing,C.H. (2003) Chromatin dynamics and locus accessibility in the immune system. *Nat. Immunol.*, **4**, 603–606.
2. de Laat,W. and Grosveld,F. (2007) Inter-chromosomal gene regulation in the mammalian cell nucleus. *Curr. Opin. Genet. Dev.*, **17**, 456–464.

3. Williams,R.R., Broad,S., Sheer,D. and Ragoussis,J. (2002) Subchromosomal positioning of the epidermal differentiation complex (EDC) in keratinocyte and lymphoblast interphase nuclei. *Exp. Cell. Res.*, **272**, 163–175.

4. Volpi,E.V., Chevret,E., Jones,T., Vatcheva,R., Williamson,J., Beck,S., Campbell,R.D., Goldsworthy,M., Powis,S.H., Ragoussis,J. et al. (2000) Large-scale chromatin organization of the major histocompatibility complex and other regions of human chromosome 6 and its response to interferon in interphase nuclei. *J. Cell Sci.*, **113(Pt 9)**, 1565–1576.

5. Morey,C., Da Silva,N.R., Perry,P. and Bickmore,W.A. (2007) Nuclear reorganisation and chromatin decondensation are conserved, but distinct, mechanisms linked to Hox gene activation. *Development*, **134**, 909–919.

6. Chambeyron,S. and Bickmore,W.A. (2004) Chromatin decondensation and nuclear reorganization of the HoxB locus upon induction of transcription. *Genes Dev.*, **18**, 1119–1130.

7. Tolhuis,B., Palstra,R.J., Splinter,E., Grosveld,F. and de Laat,W. (2002) Looping and interaction between hypersensitive sites in the active beta-globin locus. *Mol. Cell*, **10**, 1453–1465.

8. Vernimmen,D., De Gobbi,M., Sloane-Stanley,J.A., Wood,W.G. and Higgs,D.R. (2007) Long-range chromosomal interactions regulate the timing of the transition between poised and active gene expression. *EMBO J.*, **26**, 2041–2051.

9. Ni,Z., Abou El Hassan,M., Xu,Z., Yu,T. and Bremner,R. (2008) The chromatin-remodeling enzyme BRG1 coordinates CIITA induction through many interdependent distal enhancers. *Nat. Immunol.*, **9**, 785–793.

10. Barnett,D.H., Sheng,S., Charn,T.H., Waheed,A., Sly,W.S., Lin,C.Y., Liu,E.T. and Katzenellenbogen,B.S. (2008) Estrogen receptor regulation of carbonic anhydrase XII through a distal enhancer in breast cancer. *Cancer Res.*, **68**, 3505–3515.

11. Chan,P.K., Wai,A., Philipsen,S. and Tan-Un,K.C. (2008) 5′HS5 of the human beta-globin locus control region is dispensable for the formation of the beta-globin active chromatin hub. *PLoS ONE*, **3**, e2134.

12. Duan, H., Xiang, H., Ma, L. and Boxer, L.M. (2008) Functional long-range interactions of the IgH 3′ enhancers with the bcl-2 promoter region in t(14;18) lymphoma cells. *Oncogene*. **27**, 6720–6728.

13. Engel,N., Raval,A.K., Thorvaldsen,J.L. and Bartolomei,S.M. (2008) Three-dimensional conformation at the H19/Igf2 locus supports a model of enhancer tracking. *Hum. Mol. Genet.*, **17**, 3021–3029.

14. Qiu,X., Vu,T.H., Lu,Q., Ling,J.Q., Li,T., Hou,A., Wang,S.K., Chen,H.L., Hu,J.F. and Hoffman,A.R. (2008) A complex deoxyribonucleic acid looping configuration associated with the silencing of the maternal Igf2 allele. *Mol. Endocrinol.*, **22**, 1476–1488.

15. Tsai,C.L., Rowntree,R.K., Cohen,D.E. and Lee,J.T. (2008) Higher order chromatin structure at the X-inactivation center via looping DNA. *Dev. Biol.*, **319**, 416–425.

16. Xu,M. and Cook,P.R. (2008) Similar active genes cluster in specialized transcription factories. *J. Cell Biol.*, **181**, 615–623.

17. Bednar,J., Horowitz,R.A., Dubochet,J. and Woodcock,C.L. (1995) Chromatin conformation and salt-induced compaction: three-dimensional structural information from cryoelectron microscopy. *J. Cell Biol.*, **131**, 1365–1376.

18. Zlatanova,J. and Leuba,S.H. (2003) Chromatin fibers, one-at-a-time. *J. Mol. Biol.*, **331**, 1–19.

19. Solov'eva,L., Svetlova,M., Bodinski,D. and Zalensky,A.O. (2004) Nature of telomere dimers and chromosome looping in human spermatozoa. *Chromosome Res.*, **12**, 817–823.

20. Dekker,J., Rippe,K., Dekker,M. and Kleckner,N. (2002) Capturing chromosome conformation. *Science*, **295**, 1306–1311.

21. Spilianakis,C.G. and Flavell,R.A. (2004) Long-range intrachromosomal interactions in the T helper type 2 cytokine locus. *Nat. Immunol.*, **5**, 1017–1027.

22. Spilianakis,C.G., Lalioti,M.D., Town,T., Lee,G.R. and Flavell,R.A. (2005) Interchromosomal associations between alternatively expressed loci. *Nature*, **435**, 637–645.

23. Hagege,H., Klous,P., Braem,C., Splinter,E., Dekker,J., Cathala,G., de Laat,W. and Forne,T. (2007) Quantitative analysis of chromosome conformation capture assays (3C-qPCR). *Nat. Protoc.*, **2**, 1722–1733.

24. Splinter,E., Heath,H., Kooren,J., Palstra,R.J., Klous,P., Grosveld,F., Galjart,N. and de Laat,W. (2006) CTCF mediates long-range chromatin looping and local histone modification in the beta-globin locus. *Genes Dev.*, **20**, 2349–2354.

25. Wurtele,H. and Chartrand,P. (2006) Genome-wide scanning of HoxB1-associated loci in mouse ES cells using an open-ended Chromosome Conformation Capture methodology. *Chromosome Res.*, **14**, 477–495.

26. Feschotte,C. (2008) Transposable elements and the evolution of regulatory networks. *Nat. Rev. Genet.*, **9**, 397–405.

27. Britten,R.J. (1996) DNA sequence insertion and evolutionary variation in gene regulation. *Proc. Natl Acad. Sci. USA*, **93**, 9374–9377.

28. Randegger,C.C. and Hachler,H. (2001) Real-time PCR and melting curve analysis for reliable and rapid detection of SHV extended-spectrum beta-lactamases. *Antimicrob Agents Chemother.*, **45**, 1730–1736.

29. Bextine,B. and Child,B. (2007) Xylella fastidiosa genotype differentiation by SYBR Green-based QRT-PCR. *FEMS Microbiol Lett.*, **276**, 48–54.

30. Liu,Y., Zhu,Q. and Zhu,N. (2007) Rapid HLA-DR fluorotyping based on melting curve analysis. *Immunol. Invest.*, **36**, 507–521.

31. Santhosh,S.R., Parida,M.M., Dash,P.K., Pateriya,A., Pattnaik,B., Pradhan,H.K., Tripathi,N.K., Ambuj,S., Gupta,N., Saxena,P. et al. (2007) Development and evaluation of SYBR Green I-based one-step real-time RT-PCR assay for detection and quantification of Chikungunya virus. *J. Clin. Virol.*, **39**, 188–193.

32. Akey,D.T., Akey,J.M., Zhang,K. and Jin,L. (2002) Assaying DNA methylation based on high-throughput melting curve approaches. *Genomics*, **80**, 376–384.

33. Busi,F. and Cresteil,T. (2005) Phenotyping-genotyping of alternatively spliced genes in one step: study of CYP3A5*3 polymorphism. *Pharmacogenet Genomics*, **15**, 433–439.

34. Zhang,X., Caggana,M., Cutler,T.L. and Ding,X. (2004) Development of a real-time polymerase chain reaction-based method for the measurement of relative allelic expression and identification of CYP2A13 alleles with decreased expression in human lung. *J. Pharmacol. Exp. Ther.*, **311**, 373–381.

35. Aaronson,D.S. and Horvath,C.M. (2002) A road map for those who don't know JAK-STAT. *Science*, **296**, 1653–1655.

36. Maher,S.G., Romero-Weaver,A.L., Scarzello,A.J. and Gamero,A.M. (2007) Interferon: cellular executioner or white knight? *Curr. Med. Chem.*, **14**, 1279–1289.

37. LeibundGut-Landmann,S., Waldburger,J.M., Krawczyk,M., Otten,L.A., Suter,T., Fontana,A., Acha-Orbea,H. and Reith,W. (2004) Mini-review: Specificity and expression of CIITA, the master regulator of MHC class II genes. *Eur. J. Immunol.*, **34**, 1513–1525.

38. Wright,K.L. and Ting,J.P. (2006) Epigenetic regulation of MHC-II and CIITA genes. *Trends Immunol.*, **27**, 405–412.

39. Ni,Z., Karaskov,E., Yu,T., Callaghan,S.M., Der,S., Park,D.S., Xu,Z., Pattenden,S.G. and Bremner,R. (2005) Apical role for BRG1 in cytokine-induced promoter assembly. *Proc. Natl Acad. Sci. USA*, **102**, 14611–14616.

40. Palstra,R.J., Tolhuis,B., Splinter,E., Nijmeijer,R., Grosveld,F. and de Laat,W. (2003) The beta-globin nuclear compartment in development and erythroid differentiation. *Nat. Genet.*, **35**, 190–194.

41. Dekker,J. (2006) The three 'C's of chromosome conformation capture: controls, controls, controls. *Nat. Methods*, **3**, 17–21.

42. Chang,H.W., Cheng,C.A., Gu,D.L., Chang,C.C., Su,S.H., Wen,C.H., Chou,Y.C., Chou,T.C., Yao,C.T., Tsai,C.L. et al. (2008) High-throughput avian molecular sexing by SYBR green-based real-time PCR combined with melting curve analysis. *BMC Biotechnol.*, **8**, 12.

43. Jung,M., Muche,J.M., Lukowsky,A., Jung,K. and Loening,S.A. (2001) Dimethyl sulfoxide as additive in ready-to-use reaction mixtures for real-time polymerase chain reaction analysis with SYBR Green I dye. *Anal. Biochem.*, **289**, 292–295.

44. Giglio,S., Monis,P.T. and Saint,C.P. (2003) Demonstration of preferential binding of SYBR Green I to specific DNA fragments in real-time multiplex PCR. *Nucleic Acids Res.*, **31**, e136.

45. Splinter,E., Grosveld,F. and de Laat,W. (2004) 3C technology: analyzing the spatial organization of genomic loci in vivo. *Methods Enzymol.*, **375**, 493–507.

46. Pattenden,S.G., Klose,R., Karaskov,E. and Bremner,R. (2002) Interferon-gamma-induced chromatin remodeling at the CIITA locus is BRG1 dependent. *EMBO J.*, **21**, 1978–1986.

47. Dalpke,A., Heeg,K., Bartz,H. and Baetz,A. (2008) Regulation of innate immunity by suppressor of cytokine signaling (SOCS) proteins. *Immunobiology*, **213**, 225–235.

48. Gudnason,H., Dufva,M., Bang,D.D. and Wolff,A. (2007) Comparison of multiple DNA dyes for real-time PCR: effects of dye concentration and sequence composition on DNA amplification and melting temperature. *Nucleic Acids Res.*, **35**, e127.